Article

Insights Into the Properties of Amygdalin Solvatomorphs: X-ray Structures, Intermolecular Interactions, and Transformations

Tingting Zhang, Shiying Yang, Baoxi Zhang, Dezhi Yang,* Yang Lu,* and Guanhua Du*

Cite This: *ACS Omega* 2022, 7, 8906–8918

Read Online

ACCESS | Metrics & More | Article Recommendations | Supporting Information

ABSTRACT: Amygdalin is an effective component of the traditional Chinese medicine bitter almond, peach kernel, and plum kernel. It has pharmacological effects, such as relieving cough and asthma. In a study of the crystallization process, we found a series of solvatomorphs of amygdalin (including hydrate). Interestingly, in the structures of these solvatomorphs, the same characteristic structural fragment is present, that is, amygdalin dihydrate. Multiple analytical techniques were used to characterize the solvatomorphs, such as X-ray diffraction and thermogravimetry–mass spectrometry. Void calculations of water and solvent

were used to analyze the occupied volume in the unit cell of the corresponding solvatomorphs to explain the formation mechanism of the solvatomorphs from the perspective of space. To elucidate the formation mechanism of the solvatomorphs with this kind of characteristic structure from the perspective of energy, theoretical calculations based on density functional theory were applied, such as energy decomposition and molecular electrostatic potential surfaces. In addition, the transformation phenomenon between these solvatomorphs and amygdalin was identified, and the transformation pathways are described in detail.
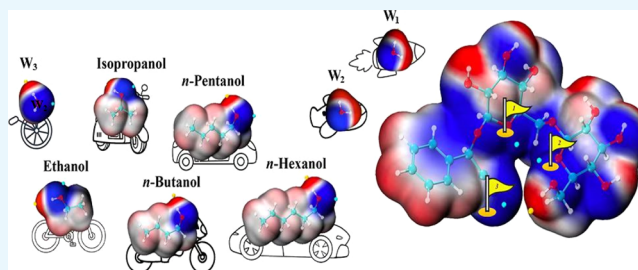
1. INTRODUCTION

Amygdalin (AMY), also known as vitamin B_{17}, is mainly found in the dried mature seeds and leaves of common Chinese medicines such as Rosaceae *Prunus armeniaca* L and *Prunus humilis*.[1,2] AMY is a cyanogenic compound in plants. When the corresponding tissues of plants are damaged by external forces or other conditions, plants release a large amount of hydrogen cyanide to protect themselves. In addition, AMY can act as a storage molecule for reduced nitrogen to a certain extent, which plays a very important role in plants.[3,4] By studying the repair effect of AMY in plants and then studying and analyzing the pharmacological effect, researchers found that AMY exhibits obvious pharmacological activities. It has become a commonly used auxiliary anticancer drug and expectorant cough agent,[5,6] and it is also used to treat asthma, bronchitis, emphysema, leprosy, colorectal cancer, leucoderma, and coagulation, and it has anti-inflammatory, neoplastic, thirst-quenching, antipyretic, and microcirculatory disturbance effects.[7−11] AMY is composed of two molecules of glucose and one molecule of aglycone. Its molecular structure is shown in Figure 1. The molecular formula is $C_{20}H_{27}O_{11}N$, and the relative molecular mass is 457.4.

For the crystallographic study of AMY, there is only one report on AMY trihydrate (AMY-W).[12] In addition, the crystallographic data of AMY ethanol dihydrate (AMY-Eth) are included in the Cambridge Crystallographic Data Centre (CCDC deposition number 1871571), although there is no literature report on its crystal structure analysis.

Solvatomorph refers to a crystalline substance formed by the combination of a compound and one or more solvent molecules
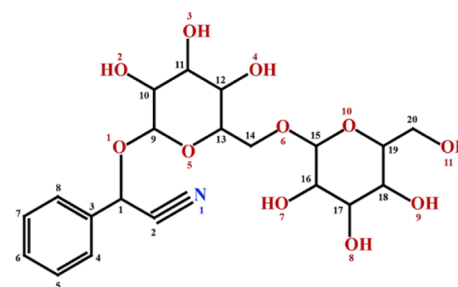

Figure 1. Chemical structure of AMY with atomic numbering (black numbers represent carbon atoms, blue numbers represent nitrogen atoms, and red numbers represent oxygen atoms).

in a crystal lattice. In the drug production process, active pharmaceutical ingredient molecules inevitably come into contact with solvent molecules, so the formation of solvatomorphs is very common during drug development.[13,14] According to statistics, approximately one-third of organic molecules can form solvatomorphs or hydrates. The most
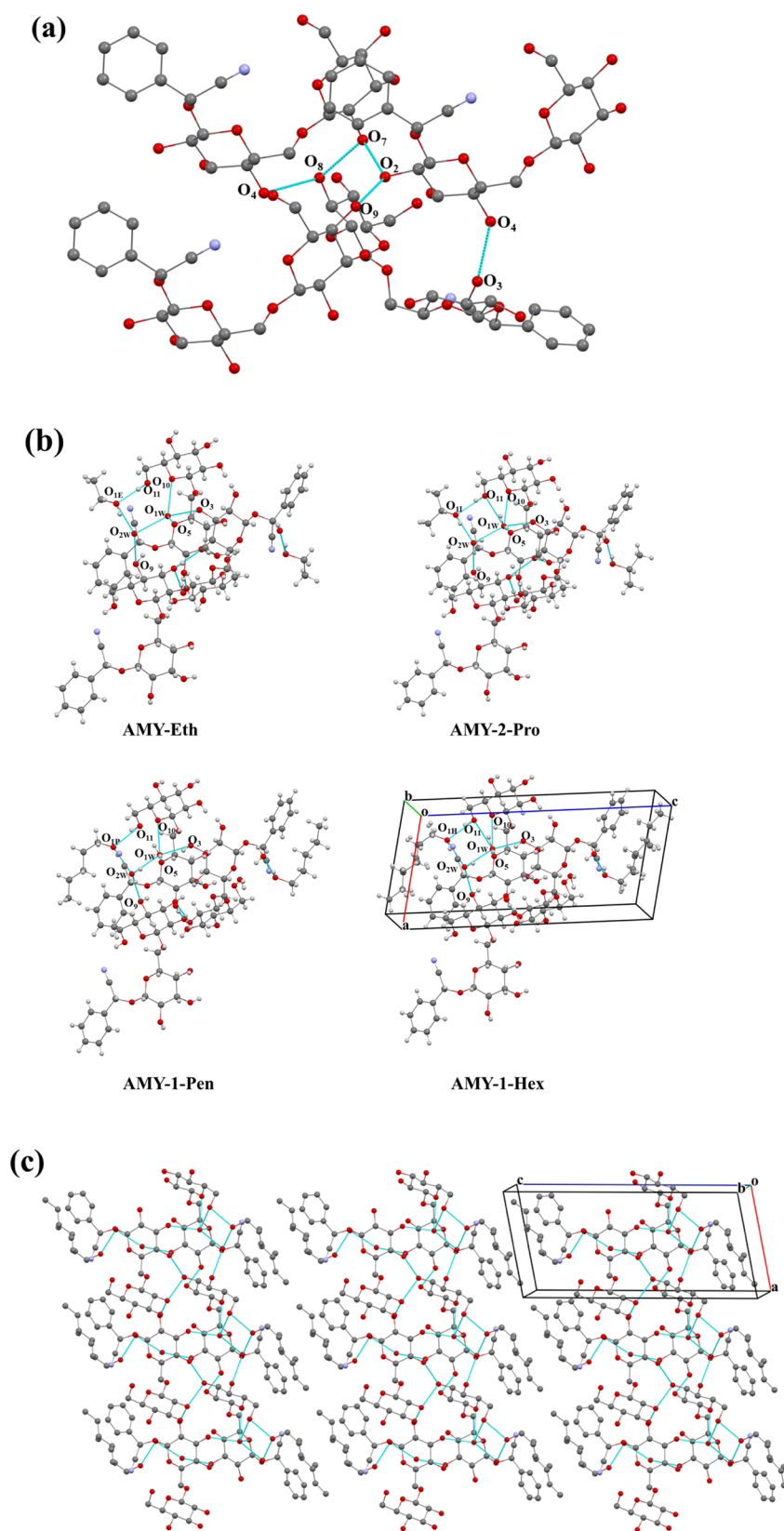
Figure 2. Part of the crystal structures for the solvatomorphs. (a) Hydrogen bonds among AMY molecules; (b) intermolecular hydrogen-bond networks of AMY-Eth, AMY-2-Pro, AMY-1-Pen, and AMY-1-Hex crystals; (c) 2D network structure constructed by the hydrogen bonds of AMY-1-Hex. Oxygen atoms are in red, carbon atoms are in grey, nitrogen atoms are in blue, and solvent molecules are drawn in the ball-and-stick model.

typical example is sulfathiazole, and more than 100 solvato-morphs have been found.[15]

During the development and purification of AMY, it was found that the compound easily formed alcohol solvatomorphs.

After a series of experiments and studies, four new solvatomorphs of AMY were prepared, namely isopropanol dihydrate (AMY-2-Pro), n-butanol dihydrate (AMY-1-But), n-pentanol dihydrate (AMY-1-Pen), and n-hexanol dihydrate (AMY-1-Hex), and their crystal data were obtained. Interestingly, all hydrate and solvatomorphs have the structural characteristics of "AMY dihydrate" as the main fragment, and as the crystallization solvent system changes, another water or solvent molecule is included in the compounds. Two water molecules in the main fragment were named W_1 and W_2 according to the distance to the host molecule, and the other included water or solvent molecules were named W_3 or S_3. As structural information derived from an X-ray diffraction (XRD) study of a single crystal is the most fundamental description of a polymorph or solvatomorph and helps to explain formation reasons for polymorphism or solvatomorphism at the atomic scale,[16] six crystalline forms (AMY-W, AMY-Eth, AMY-2-Pro, AMY-1-But, AMY-1-Pen, and AMY-1-Hex) are analyzed in the present work, and similarity occurs among these solvatomorphs. The crystal structures and hydrogen bond interactions of these six crystal forms were analyzed.

The six solvatomorphs were characterized by multiple methods, including single-crystal XRD (SXRD), powder XRD (PXRD), Fourier transform-infrared spectroscopy, thermal analysis, and water solubility. Thermal analysis is an important method to study solvatomorphs. There are several kinds of thermal analysis technology, and the most common are thermogravimetric analysis (TG) and differential scanning calorimetry (DSC). In addition, the normal thermogravimetry−mass spectrometry (TG−MS) coupling analysis system has been considered a powerful hyphenated technique for evolved gas analysis.[17] Compared with the SXRD method, TG−MS analysis provides more flexible requirements for the samples, particularly those solvatomorphs that hardly form as single crystals, which are suited for SXRD experiments. Previous researchers have also reported the use of the TG−MS method to analyze and characterize solvatomorphs.[18−20] The six crystal forms were characterized by thermal analysis, including TG, DSC, and TG−MS.

In this study, theoretical calculations based on density function theory (DFT) were used to explain the mechanism underlying the special crystallization style.[21,22] The principal intermolecular interactions between molecules were analyzed by using the energy decomposition analysis (EDA) method based on symmetry-adapted perturbation theory (SAPT), and the interaction sites were explained by using the molecular electrostatic potential surface (MEPS).[23] In addition, contact and solvent accessible surface analysis, Xpac analysis, and Hirshfeld surface analysis were also applied to elucidate the formation mechanism of the series of solvatomorphs.

Finally, based on the above research, crystal transformation was also investigated.[24,25] There were transformation pathways among AMY, AMY-W, and AMY alcohol dihydrates, which was consistent with the results of theoretical calculations. The single-crystal structures of AMY alcohol dihydrates (AMY-2-Pro, AMY-1-But, AMY-1-Pen, and AMY-1-Hex) have been reported for the first time.

2. RESULTS AND DISCUSSION

2.1. SXRD Analysis. Six prism crystals suitable for crystal structure determination by SXRD were obtained from their respective solutions by slow evaporation. The chemical, crystallographic, and refinement parameters of solvatomorphs

are listed in Table S1. Crystallographic data for solvatomorphs AMY-2-Pro, AMY-1-Pen, and AMY-1-Hex were deposited at the Cambridge Crystallographic Data Centre, and the deposition numbers were 2128815, 2128827, 2128825, respectively. AMY molecules in a unit cell were arranged loosely, leading to relatively low-density values (approximately 1.3 g/cm^3) compared with those of other solid-state crystalline compounds. Except for AMY-Eth, the other solvatomorphs showed an approximate volume of approximately 1200 Å^3, which increased with the solvent volume.

There were two space groups in AMY solvatomorphs, the monoclinic $P2_1$ space group (AMY-W, AMY-2-Pro, AMY-1-But, AMY-1-Pen, and AMY-1-Hex) and the orthorhombic $P2_12_12_1$ space group (AMY-Eth). Isostructurality[26] was found among solvatomorphs of $P2_1$ groups with similar unit cell parameters, crystal packing, and hydrogen-bonding interaction styles in the respective unit cells.

In the series of AMY alcohol dihydrate solvatomorphs (AMY-Eth, AMY-2-Pro, AMY-1-But, AMY-1-Pen, and AMY-1-Hex), alcohol molecules were located at the edge of the crystal cell. In the a and b axis directions, AMY played a leading role in the lengths of a and b, and the extension of the alcohol carbon chain did not affect the spatial structure in the a and b axis directions. Therefore, the a and b parameters of all AMY alcohol dihydrate solvatomorphs were almost the same. With the growth of the carbon chain in alcohol molecules, the space required for the alcohol solvent in the c-axis direction increased, so the parameters c and β angle of the AMY alcohol dihydrate solvatomorphs increased with the extension of the alcohol carbon chains. AMY-Eth belonged to the orthorhombic system, and the β angle was 90°. The β angles of AMY-2-Pro, AMY-1-But, AMY-1-Pen, and AMY-1-Hex were greater than 90°, and they belonged to the monoclinic system. For AMY-W, the volume of water molecules was small and had little effect on the space arrangement. The crystal units of AMY-1-Hex are shown in Figure 2b.

2.2. Hydrogen-Bonding Interaction. AMY is a poly-hydroxy compound. All hydroxyl groups in the AMY molecule participated in the formation of hydrogen bonds. The AMY molecules are connected through the hydrogen-bond interactions of $O_2-H_2\cdots O_7$, $O_4-H_4\cdots O_3$, $O_7-H_7\cdots O_8$, $O_8-H_8\cdots O_4$, and $O_9-H_9\cdots O_2$ (Figure 2a). O_1 and O_6 atoms were not involved in the formation of classical hydrogen bonds. The six solvatomorphs of AMY exhibited similar intermolecular arrangements. The solvents interacted with the host molecules through hydrogen bonds, making the whole spatial structure more compact. Conventional hydrogen bonds via O−H⋯O were major interactions in the solvatomorphs studied in this work.[27] Intermolecular hydrogen-bond networks of AMY-Eth, AMY-2-Pro, AMY-1-Pen, and AMY-1-Hex crystals were provided in Figure 2b.

The following analysis took AMY-1-Hex as an example. In the crystal unit, AMY was connected with water molecule W_1 through the $O_{1W}-H_{1WB}\cdots O_{11}$ hydrogen bond, W_1 was connected with water molecule W_2 through the $O_{2W}-H_{2WB}\cdots O_{1W}$ hydrogen bond, W_2 was connected with isopropanol through the $O_{1H}-H_{1H}\cdots O_{2W}$ hydrogen bond, and the isopropanol molecule was connected with AMY through the $O_{11}-H_{11}\cdots O_{1H}$ hydrogen bond (Figure 2b), forming a four-membered ring structure. The unit cell molecules were arranged in the same hydrogen-bond connection mode: under the interaction of $O_{2W}-H_{2WA}\cdots O_9$, two hydrogen bond chains along the a-axis were formed. Then, the two adjacent chains formed a

two-dimensional (2D)-layered structure in the ac plane through the $O_3-H_3\cdots O_{1W}$ hydrogen-bond interaction. The layers were stacked by van der Waals forces, and no hydrogen bond connection was found (Figure 2c). Along the c-axis, AMY molecules were connected by the $O_{1W}-H_{1WA}\cdots O_5$ hydrogen bond to finally form a three-dimensional structure. It should be noted that the hydrogen-bond interactions of AMY-Eth (ethanol dihydrate) were consistent with those of monoclinic forms (AMY-W, AMY-2-Pro, AMY-1-But, AMY-1-Pen, and AMY-1-Hex), except that the a and b axes needed to be exchanged for analysis.

Isomorphism[28] exists among six solvatomorphs, which have similar crystalline properties and hydrogen bondings. Although the crystallographic data of AMY-1-But were not good enough to be deposited with CCDC, the basic structure information was clear and could be used for crystal structure analysis and subsequent theoretical computation. The chemical formula, crystallographic, and refinement parameters of AMY-1-But are listed in Table S1.

2.3. PXRD Analysis. The six crystal forms were determined by the PXRD method. All displayed peaks in the measured patterns of the samples matched well with those simulated patterns generated from the corresponding SXRD data, which are shown in Figure 3a. The PXRD patterns were compared with each other, and the 2θ of the six solvatomorphs had the following features: (1) the strongest peak of each solvatomorph was the first peak, and its range of 2θ was within 10°; (2) with the increase in carbon atoms in compounds, the 2θ of the strongest peak decreased (Figure 3b).

2.4. Thermal Analysis. The thermal analysis results of the solvatomorphs of AMY are shown in Figure 4. The total amount of solvents (including W_1, W_2, W_3, or S_3) in the solvatomorphs was confirmed by calculating the mass loss from TG analysis. The determined values of mass loss (w/w) were 9.891% (AMY-W), 15.02% (AMY-Eth), 17.35% (AMY-2-Pro), 17.70% (AMY-1-But), 19.11% (AMY-1-Pen), and 22.08% (AMY-1-Hex), corresponding to calculated stoichiometric ratios (guest/host) of 0.94 (AMY-W), 0.99 (AMY-Eth), 1.00 (AMY-2-Pro), 0.91 (AMY-1-But), 0.90 (AMY-1-Pen), and 0.95 (AMY-1-Hex), respectively. TG calculation results are shown in Table S3.

The DSC curves showed that there was an obvious endothermic peak near 225 °C with no obvious weight loss, indicating that the solvatomorphs melted at this temperature. There was at least one obvious weight loss step and corresponding DSC endothermic peak in the temperature range of 35−150 °C, indicating the loss of crystalline solvents.

The six solvatomorphs were also analyzed by TG−MS. The characteristic ion peaks of the corresponding solvents could be detected at the corresponding position of the TG weight loss steps. In the SIM chromatogram of each solvatomorph, the sensitivity of the water peak was low, but the characteristic ion peaks of each alcohol solvent could be observed, which confirmed that each solvatomorph did contain the corresponding alcohol solvent.

2.5. Equilibrium Solubility in Water. Solubility is one of the most important preformulation properties, and it has a noteworthy effect on drugs, especially on their bioavailability.[29] In the present study, water was used for the solubility experiment. The solubility of AMY solvatomorphs in water at 37 °C was as follows: 4.30 mg/mL for AMY-W, 11.36 mg/mL for AMY-Eth, 6.96 mg/mL for AMY-2-Pro, 9.32 mg/mL for AMY-1-But, 7.74 mg/mL for AMY-1-Pen, and 9.86 mg/mL for AMY-1-Hex. In addition, the solubility of AMY was 7.72 mg/ml.
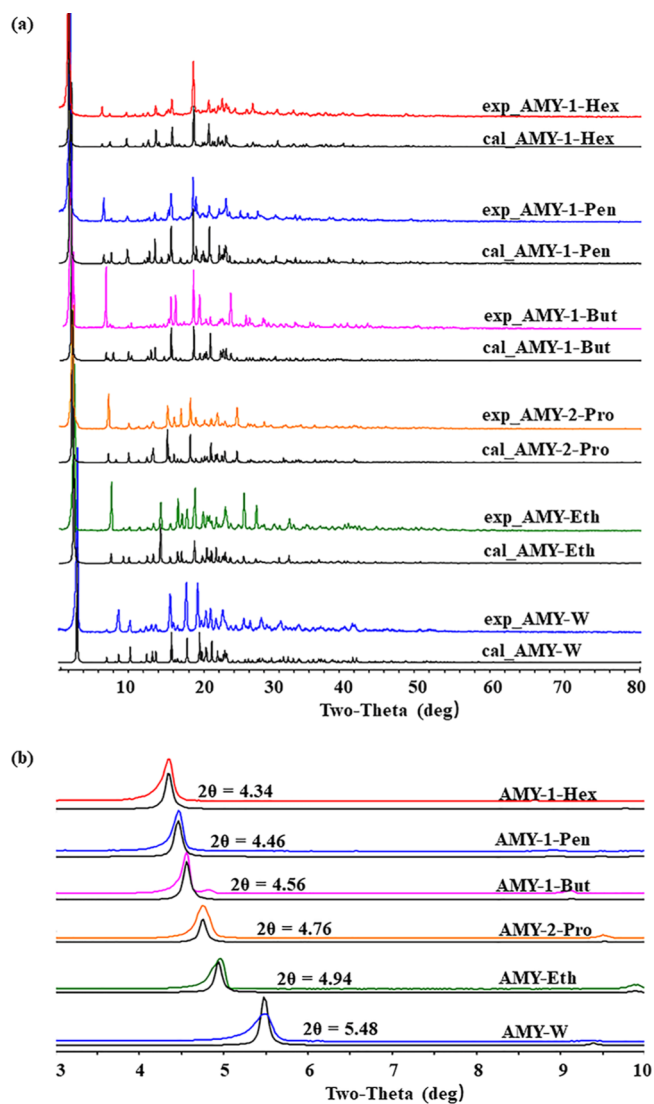

Figure 3. (a) PXRD patterns of AMY solvatomorphs. (b) Expanded region of $2\theta = 3-10°$.

All of the AMY alcohol dihydrates showed a far better solubility than AMY-W. Moreover, the solubilities of AMY-Eth, AMY-1-But, and AMY-1-Hex were better than that of AMY.

2.6. Theoretical Computation. *2.6.1. Contact and Solvent-Accessible Surface Analysis.* In this paper, we calculated the voids of the six solvatomorphs using a contact surface and solvent-accessible surface to estimate the volume that could be filled by water and solvent molecules. The surface of the W_1 molecule is mapped in red, the W_2 molecule in cyan, and the W_3 or S_3 molecule in purple. The results are listed in Table 1. The statistical results and the surfaces of AMY-2-Pro as an example are presented in Figure 5, and contact surfaces and solvent-accessible surfaces of the other five solvatomorphs are presented in Figure S1. Judging from the contact surface and solvent-accessible surface, the void volume near the center of the AMY molecule is small, with mean values of 135 and 14 $Å^3$, respectively. Based on the analysis above, it is speculated that since the volume occupied by all of the other solvent molecules is larger than that of the water molecule, this space could only be occupied by water. This may explain the formation of the AMY dihydrate fragment rather than other solvent complex fragments.
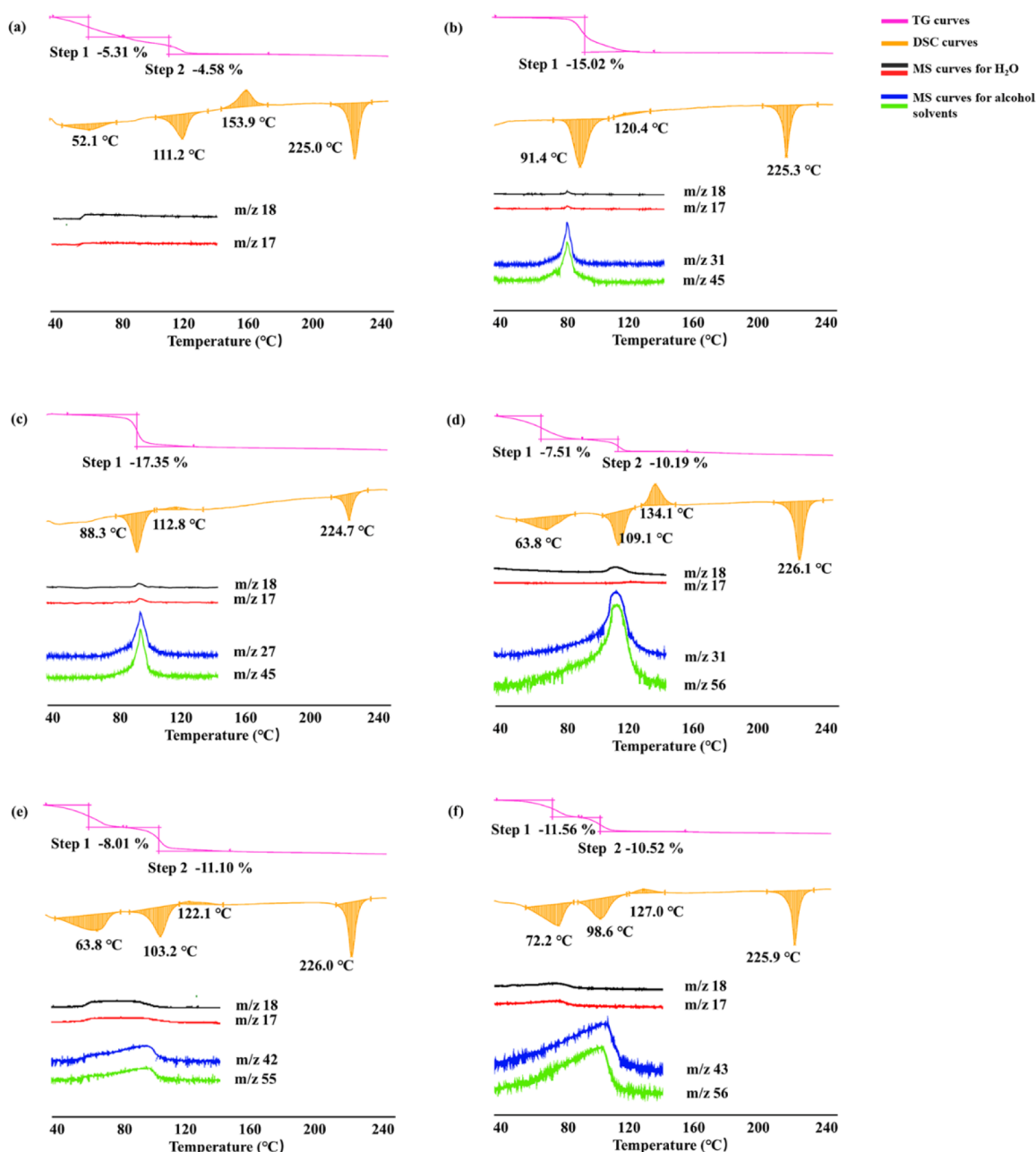
Figure 4. TG, DSC, and MS characteristic ion curves of solvatomorphs (a) AMY-W, (b) AMY-Eth, (c) AMY-2-Pro, (d) AMY-1-But, (e) AMY-1-Pen, and (f) AMY-1-Hex.

2.6.2. Interaction Energies and EDA. We extracted the molecules according to the H-bond interaction to evaluate the interaction energy between water or solvent molecules and other molecules in an asymmetric unit and carried out EDA. The results are listed in Tables S4–S6. And the results of the pairwise interaction analysis[30] are listed in Table 2. The EDA results of different solvatomorphs are shown in Figure 6. The interaction energy of W_1 is the strongest, with a mean value of approximately −21.22 kcal/mol. The interaction energy of W_2 is weaker than that of W_1, with a mean value of approximately −18.23 kcal/mol. The interaction energy of W_3 or S_3 is the weakest, with a mean value of approximately −16.66 kcal/mol. The results showed that the interaction energies between W_1 or W_2 and surrounding molecules are stronger than those between W_3 or S_3 and surrounding molecules in these solvatomorphs, which elucidated the rationality of the main structural

fragment—AMY dihydrate (composed of AMY and two water molecules)—from an energy perspective. By comparing the interaction energy of W_3 and S_3 with the main structural fragment of AMY dihydrate, we found that the interaction energy of W_3 is the smallest while S_3 is higher, which can reasonably explain the formation of different solvatomorphs rather than the formation of trihydrate when they crystallize in different alcohol solutions.

EDA based on SAPT can decompose the interaction energy into four different physical components to understand the nature of the interaction from an energy perspective. The four energies are electrostatic energy, exchange energy, dispersion energy, and induction energy.[31] The results showed that the main interaction between water or solvent molecules and other molecules is the electrostatic attraction effect. Induction and dispersion, as attraction effects, although small, play non-

Table 1. Contact and Solvent-Accessible Surfaces of Water and Other Solvent (W_3 or S_3) Molecules

		contact surface	solvent-accessible surface
AMY-W	W_1	125.10 (10.5%)	7.16 (0.6%)
	W_2	131.16 (11.0%)	12.08 (1.0%)
	W_3	134.34 (11.2%)	13.55 (1.1%)
AMY-Eth	W_1	247.86 (9.6%)	25.73 (1.0%)
	W_2	220.07 (8.5%)	25.10 (1.0%)
	S_3	481.94 (18.6%)	203.88 (7.9%)
AMY-2-Pro	W_1	142.10 (10.2%)	15.47 (1.1%)
	W_2	149.82 (10.8%)	19.19 (1.4%)
	S_3	330.93 (23.8%)	154.24 (11.1%)
AMY-1-But	W_1	168.02 (11.6%)	22.65 (1.6%)
	W_2	170.83 (11.8%)	24.64 (1.7%)
	S_3	399.03 (27.6%)	209.00 (14.4%)
AMY-1-Pen	W_1	141.83 (9.6%)	9.90 (0.7%)
	W_2	147.84 (10.0%)	13.76 (0.9%)
	S_3	441.92 (29.8)	253.46 (17.1%)
AMY-1-Hex	W_1	100.28 (6.6%)	5.97 (0.4%)
	W_2	109.54 (7.2%)	8.98 (0.6%)
	S_3	478.36 (31.4%)	295.70 (19.4%)

Table 2. Pairwise Counterpoise-Corrected Interaction Energies (kcal/mol) of AMY Solvatomorphs[a]

Pair	AMY-W	AMY-Eth	AMY-2-Pro	AMY-1-But	AMY-1-Pen	AMY-1-Hex
1, 2	−11.30	−11.89	−12.17	−12.21	−11.97	−11.95
1, 3	−4.44	−4.60	−4.32	−4.12	−4.20	−4.12
1, 4	−6.19	−7.17	−7.78	−7.35	−7.88	−7.48
2, 3	−5.34	−5.24	−5.11	−5.08	−5.16	−5.15
2, 4	−1.31	−1.40	−1.39	−1.28	−1.26	−1.22
3, 4	−4.84	−4.41	−5.02	−5.34	−5.29	−5.45

[a]Pair 1,2 represent AMY and W_1; pair 1,3 represent AMY and W_2; pair 1,4 represent AMY and W_3 or S_3; pair 2,3 represent W_1 and W_2; pair 2,4 represent W_1 and W_3 or S_3; pair 3,4 represent W_2 and W_3 or S_3.

negligible auxiliary roles. Exchange energy represents the repulsive force generated by proximity between molecules.

2.6.3. MEPS Analysis. The MEPS is an important tool to understand solvatomorph formation for the ability to reveal the style of intermolecular interactions.[32−34] Figure 7 presents the MEPS maps of the six investigated solvatomorphs. In the MEPS maps, blue represents the electron-rich region, red represents the electron-poor region, and white represents the neutral region. The local maxima and minima values on the MEPS are represented with yellow and cyan balls on the diagram, respectively. Following the rule that electrostatic interactions are generally generated between the local maximum value point and the local minimum value point, in the formation process of

the main structural fragment, two local maximum value points of W_1 (+44.10 and +44.00 kcal/mol, respectively) interacted with two local minimum value point of AMY molecule (−52.40 and −45.93 kcal/mol, respectively), and one of the local maximum value points of W_2 (+44.29 kcal/mol) interacted with the local minimum value point of W_1 (−37.10 kcal/mol). Then, in the formation of each solvatomorph, the local maximum and minimum value points of the main structural fragment (−47.08 and +31.27 kcal/mol, respectively) interact with the local minimum and maximum value points of water or different solvent molecules, respectively.

From the results of MEPS analysis, we found that in the process of the formation of the main structural fragment of AMY dihydrate, local minimum and maximum values of W_1, W_2, and AMY are higher than those of the solvent molecule and AMY dihydrate in the process of the formation of different solvatomorphs, which confirmed the result of the interaction energy analysis showing that W_1 and W_2 interact more strongly with AMY than W_3 and S_3.
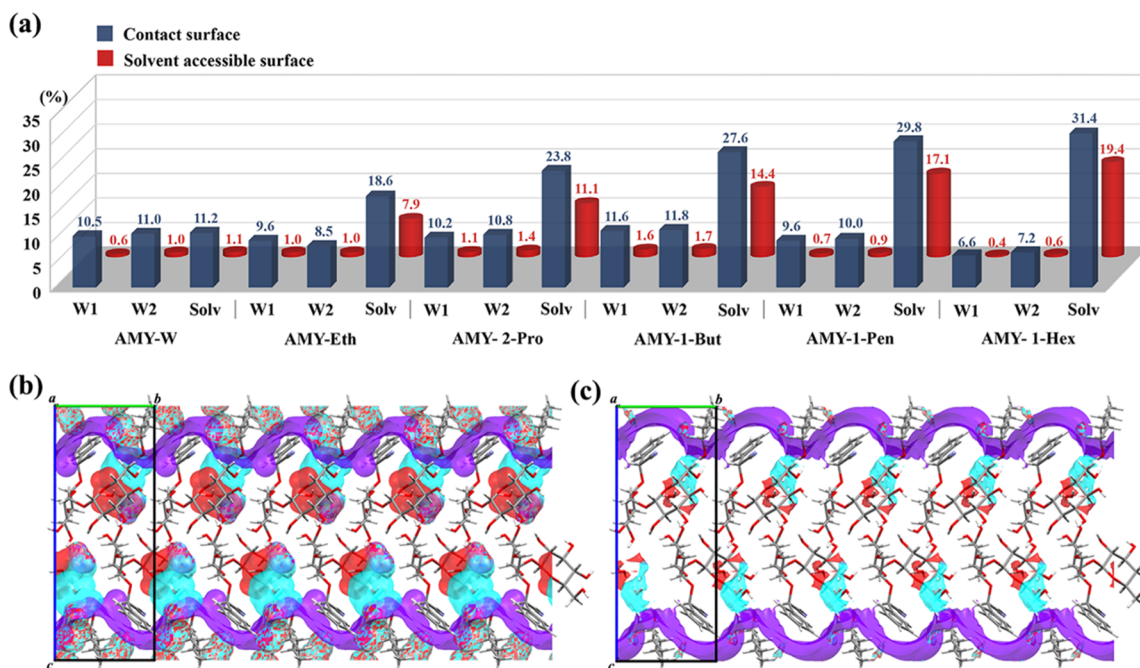

Figure 5. Contact and solvent-accessible surfaces of AMY solvatomorphs. W_1 is in red, W_2 is in cyan, and W_3 or S_3 is in purple. (a) 3-dimensional histogram of the total statistical results; (b) contact surface of AMY-2-Pro; (c) solvent-accessible surface of AMY-2-Pro.
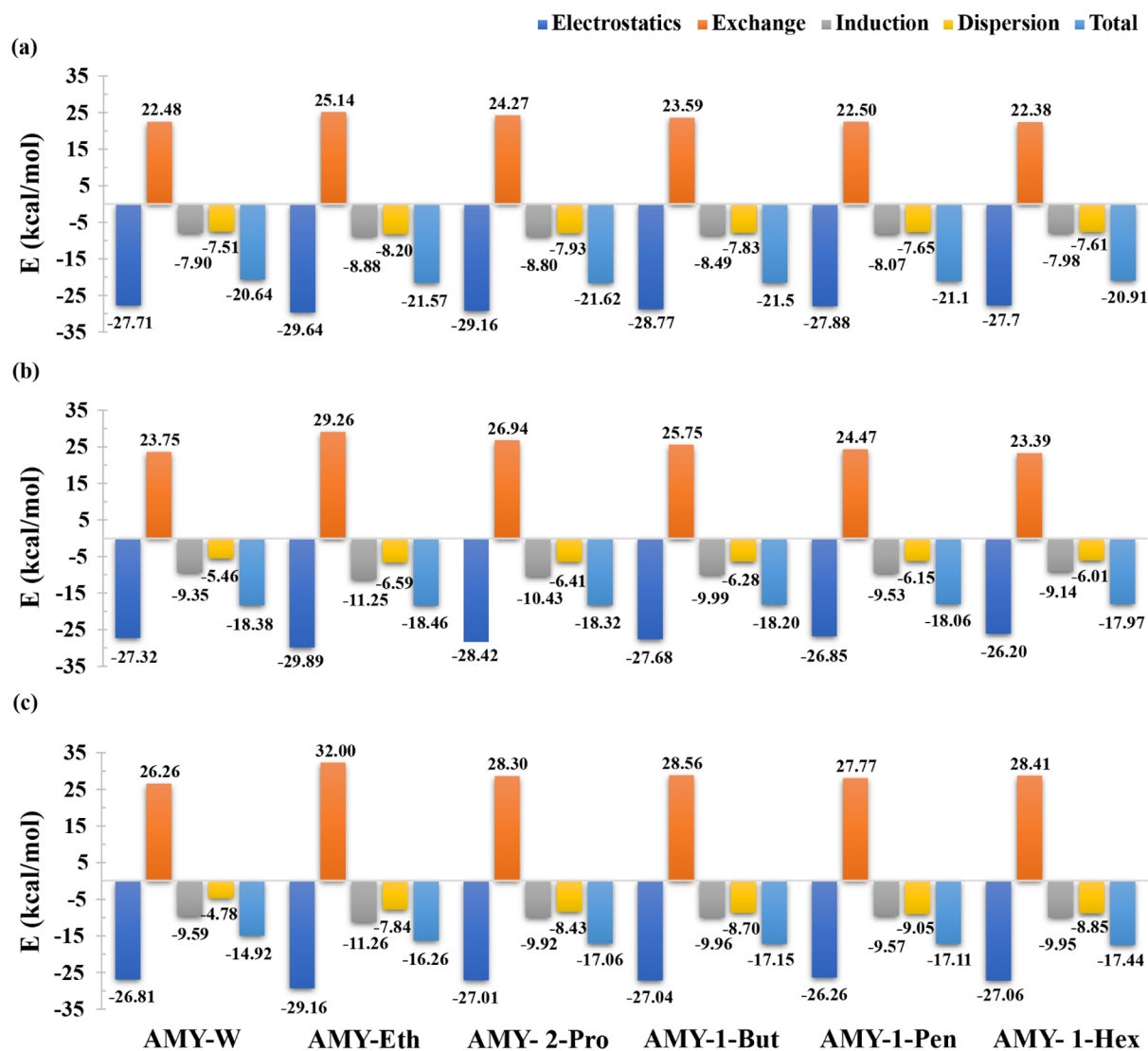
Figure 6. EDA of the intermolecular interaction in different AMY solvatomorphs. (a) Interaction energies and EDA of W_1; (b) interaction energies and EDA of W_2; (c) interaction energies and EDA of W_3 and S_3.

In the process of combining with various solvents to form solvent complexes, although the extreme point of the electrostatic potential on the surface of the water molecule is larger than that of the solvent complex, it is reasonable to consider the contribution of other energies, such as dispersion energy.

In addition, although the extremity of the water molecule on MEPS is larger than that of solvent molecules in the process of solvatomorph formation when considering the contribution of other energies, such as dispersion energy, the results are reasonable. This also suggests that a comprehensive analysis of multiple calculation methods is needed to ensure the accuracy of the conclusion.

2.6.4. XPac Analysis. The Xpac analysis was also carried out. Table 3 and Figure 8 showed information about the extent of dissimilarity (dissimilarity index x) as well as the dissimilarity parameters (stretch parameter, change in angles, and planes) between crystal structures of AMY-W and other AMY solvatomorphs. The corresponding calculations of other AMY solvatomorphs were listed in Tables S7−S10 in the Supporting Information. For XPac analysis, except for the hydrogen atoms, all the atomic coordinates in crystal geometry were taken.

2.6.5. Hirshfeld Surface Investigation. Hirshfeld surface analysis can clearly clarify the bond energy relationship within and between molecules. It is a visualization tool for studying crystal structure, and its calculation is based on electron cloud density.[35−37] Surfaces for the AMY solvatomorphs were shown in Figure 9a. The deep red spots indicated sites where hydrogen bonds were formed. It could be seen that the hydrogen bonds were mainly produced near the hydroxyl of AMY and solvent molecules. The 2D fingerprint of the solvatomorphs is shown in Figure 9b. The interaction between H···O/N/F was a hydrogen-bond donor (de > di), while the interaction between O/N/F···H was a hydrogen-bond receptor (de < di). H···O force and O···H force were the main components of the full spectrum.

As can be seen from Figure 10, among the contributions of different interactions in the process of molecular stacking, H···H was the most important intermolecular interaction, followed by O···H, and finally C···H and N···H. There were multiple hydrogen bonds in the six solvatomorphs, and hydrogen bonding existed in the formation of 2D structure and three-dimensional structure. Therefore, hydrogen bonds occupied a dominant position in the AMY solvatomorphs.
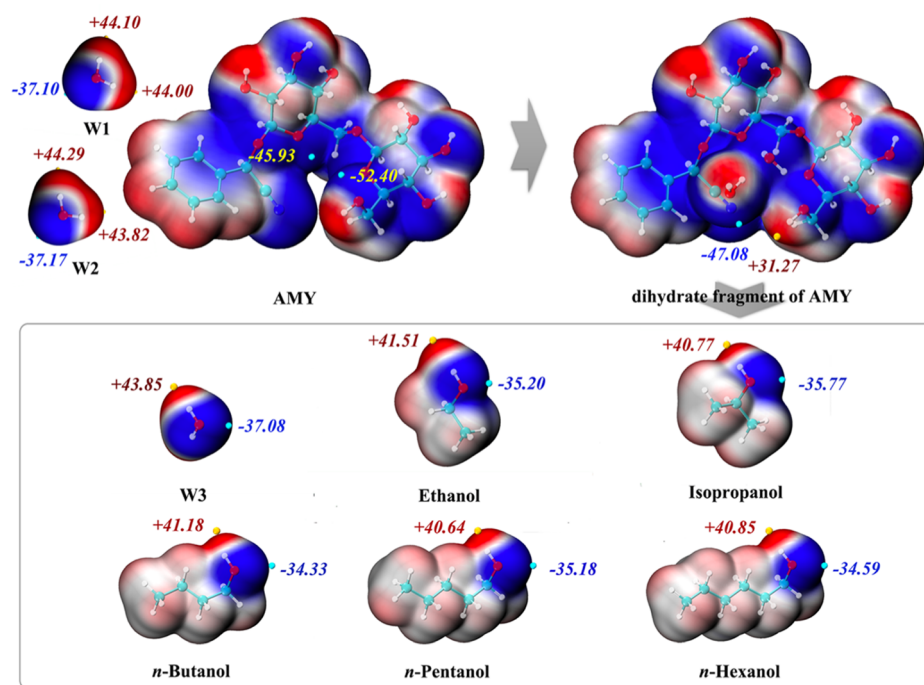
Figure 7. MEPS mapped onto the electron density isosurface of AMY and AMY solvatomorphs.

Table 3. XPac Analysis Results of Different Solvatomorphs with AMY-W

parameter	AMY-W			
	AMY-Eth	AMY-2-Pro	AMY-1-Pen	AMY-1-Hex
dissimilarity index	2.4	2.8	2.2	2.2
stretch parameter (Å)	0.06	0.06	0.05	0.05
neighbours, n	10	10	10	10
points	32	32	32	32
$\Delta[a]$ (angles) (degree)	1.1	1.3	0.9	0.9
$\Delta[p]$ (planes) (degree)	2.1	1.3	1.9	2.0

2.7. Transformation Test. The solvatomorphs of AMY in this work crystallized three molecules of solvents, including two molecules of water (W_1 and W_2) and one molecule of solvent W_3 or S_3 containing an −OH group. The structure of W_3 or S_3 can be divided into two parts: −OH and −R (the R part of trihydrate is a hydrogen atom, and the R part of alcohol dihydrate is a hydrocarbon group). All atoms in water molecules W_1 and W_2 participated in the formation of hydrogen bonds (Table S2) and firmly maintained the crystal structure. The W_3 or S_3 molecule only provided −OH to participate in hydrogen bonds, and the rest of the structure did not participate in hydrogen bonds. In addition, W_3 or S_3 molecules were arranged at the edge of the crystal structure and did not go deep into the crystal structure (Figure 2). Thus, the third molecular solvents, W_3 and S_3, may replace each other between water and alcohol.

The transformation test was carried out, and the test results were analyzed by PXRD. AMY alcohol dihydrates (AMY-Eth, AMY-2-Pro, AMY-1-But, AMY-1-Pen, and AMY-1-Hex) could be transformed into AMY-W by grinding or stirring with water, and AMY-W could also be transformed into AMY alcohol dihydrate after grinding or stirring with the corresponding alcohol solvent. That is, the transformation among the AMY solvatomorphs above was investigated (Figure 11), indicating that the force between the third solvent W_3 or S_3 and AMY and

water molecules (W_1 and W_2) was not strong, which was also consistent with the conclusion of hydrogen-bonding inter-actions and theoretical computations.

In addition, on the DSC curves of the six solvatomorphs (Figure 4), there was an exothermic peak after the endothermic peaks of desolvation, indicating that the solvatomorphs were exothermic and crystalline after desolvation. Then, each solvatomorph was heated at the end of the exothermic peak, that is, 170 °C for 10 min, measured TG and DSC, and they were transformed into AMY.

The transformation relationship of different AMY forms is very significant in the manufacturing process.[38] AMY has a high propensity to form solvatomorphs, and the recrystallized conditions in most solvents need to be controlled carefully when the no-solvent form is the desired product. This also suggests that if new alcohols, such as *n*-octanol, are used, the corresponding AMY alcohol dihydrates may also be formed.

3. CONCLUSIONS

In this paper, the crystal structures of six solvatomorphs of AMY, including AMY-W, AMY-Eth, AMY-2-Pro, AMY-1-But, AMY-1-Pen, and AMY-1-Hex, with similar structural characteristics, were systematically analyzed. Among them, AMY-2-Pro, AMY-1-But, AMY-1-Pen, and AMY-1-Hex were reported for the first time. The above six solvatomorphs were characterized by PXRD, IR, DSC, TG, and TG−MS, as well as the water solubilities. The solvatomorphs of AMY show almost no difference in the infrared spectrum, and the relevant spectra and experimental parts are shown in the Supporting Information. The six solvatomorphs were stoichiometric solvent compounds, and the ratio of AMY/water/solvent in each solvatomorph was 1:2:1. All hydroxyl groups of the six solvatomorphs participated in the formation of hydrogen bondings, and the Hirshfeld surface analysis confirmed that the O⋯H/H⋯O was the main intermolecular interaction. In addition, it was found that although the space group of AMY-Eth
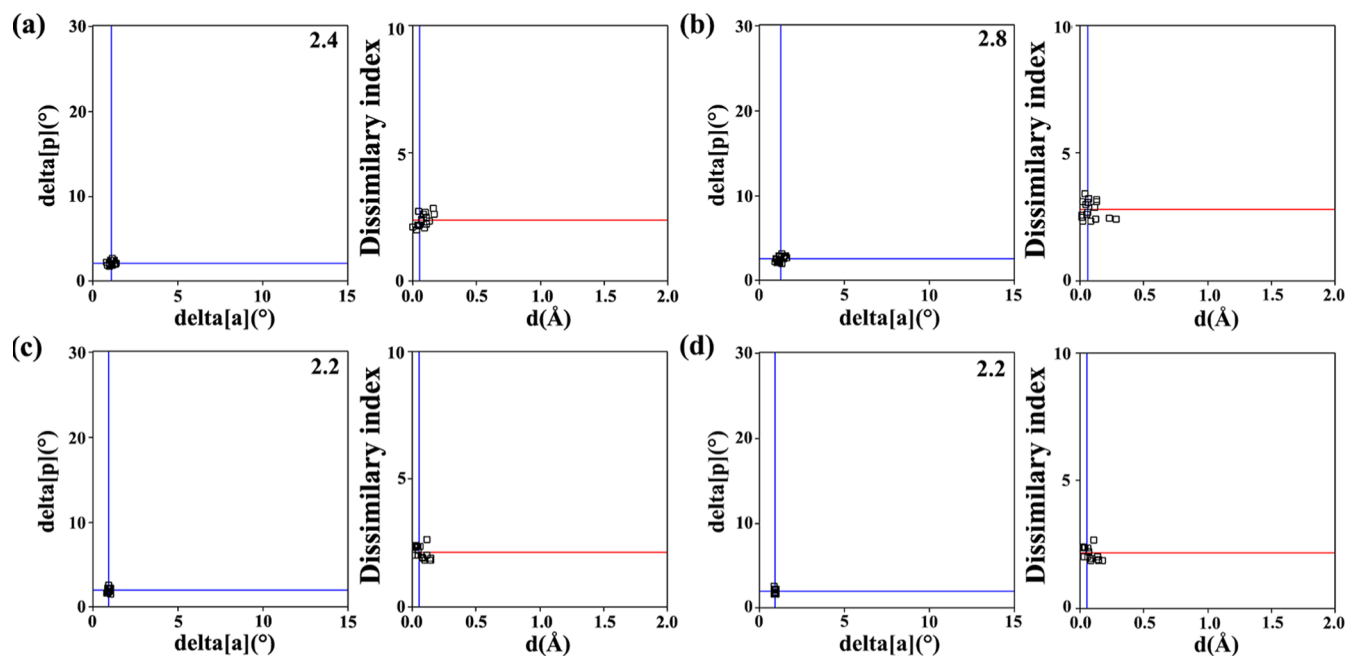
Figure 8. XPac analysis results of different solvatomorphs with AMY-W. (a) Comparison results of AMY-Eth with AMY-W; (b) comparison results of AMY-2-Pro with AMY-W; (c) comparison results of AMY-1-Pen with AMY-W; (d) comparison results of AMY-1-Hex with AMY-W.
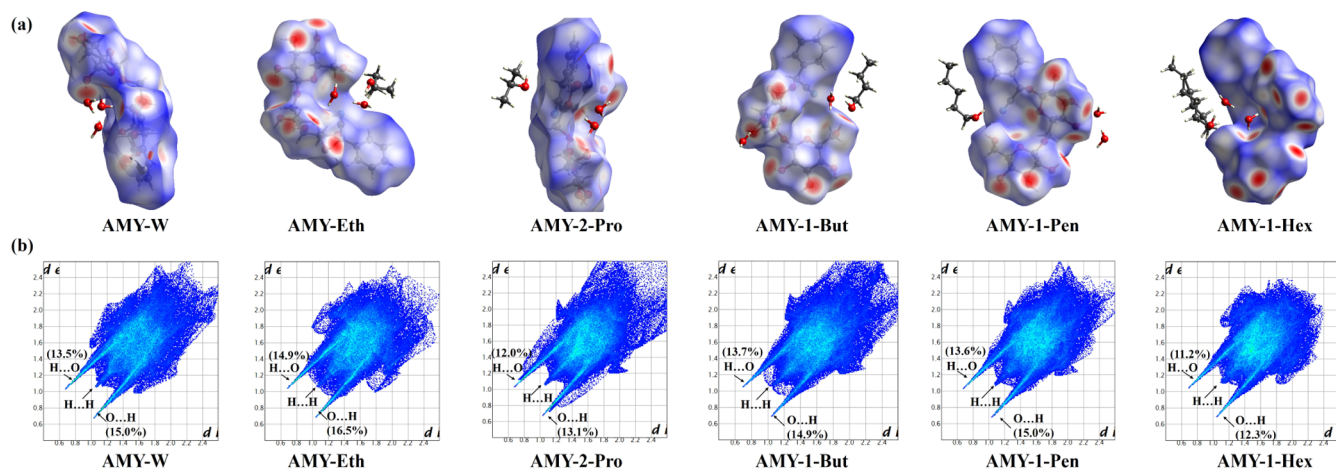

Figure 9. (a) Hirshfeld surface and (b) 2D fingerprint plots of AMY solvatomorphs.
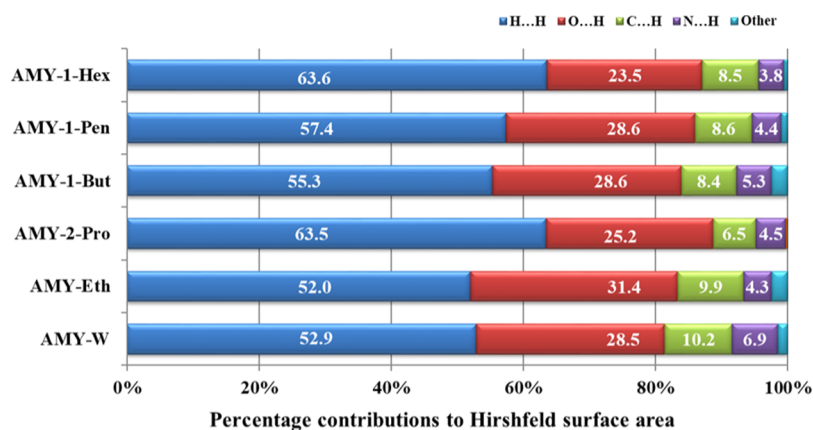

Figure 10. Contribution of different interactions to the Hirshfeld surface of AMY solvatomorphs.

(ethanol dihydrate) was different from other solvatomorphs, the hydrogen bonding and three-dimensional structure were the same as other solvatomorphs. This paper also explained the rationality of this phenomenon.
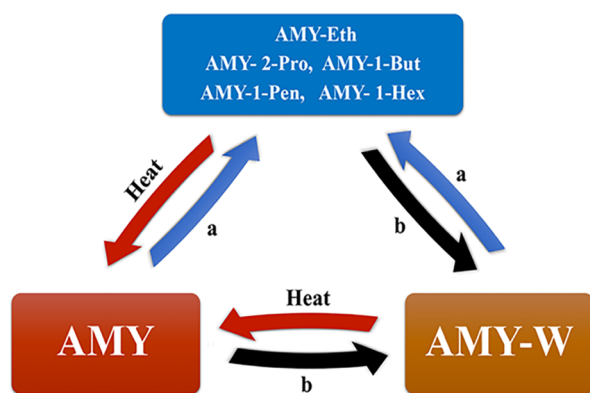
Figure 11. Transformation pathways for AMY forms. Test conditions: (a) grinding or stirring with alcohol—acetonitrile (1:1) mixed solvent; (b) grinding or stirring with water—acetonitrile (1:1) mixed solvent.

Water and alcohol solvents are polar protic solvents that function as both proton acceptors and donors. The solvents formed hydrogen bonds with AMY molecules, and then the chain structure was orderly arranged and stacked into a three-dimensional structure. Using theoretical calculations based on DFT, the mechanism of forming the characteristic structure is analyzed at the molecular level. The two water molecules were firmly combined in the crystal, connecting the alcohol solvent to the guest, while the alcohol solvents were loosely stacked at the edge of the crystal structure. Therefore, in the transformation test, solvent W_3 or S_3 was replaced, and the two water molecules (W_1 and W_2) were retained.

This article summarized the crystal structure characteristics of trihydrate and alcohol dihydrates of AMY, deepened the understanding of the crystallographic properties of AMY, and provided a reference for the design, selection, and optimization of the crystallization process of this compound. In addition, AMY easily formed corresponding dihydrate alcohol solvatomorphs when changing different alcohol solvents, and the solvatomorphs can be transformed into each other, which should be considered in drug research and the development of AMY.

4. EXPERIMENTAL SECTION

4.1. Materials. AMY (purity > 98.5%) was purchased from Nanjing Zelang Zhiti Technology Company Ltd. (batch number: 20110614; Jiangsu, China). Analytical grade solvents were obtained from Sinopharm Chemical Reagent Beijing Co., Ltd. Water was purified by a Milli-Q Reagent system (Millipore, MA, USA).

4.2. Preparation of AMY Solvatomorphs. The AMY samples were separately dissolved in water—acetonitrile mixture (1:3, v/v), ethanol, isopropanol—acetonitrile mixture (1:3, v/v), n-butanol—acetonitrile mixture (1:3, v/v), n-pentanol—acetonitrile mixture (1:3, v/v), and n-hexanol—acetonitrile mixture (1:3, v/v) and evaporated slowly at 20 °C for approximately 40 days. The single crystals obtained were named AMY-W, AMY-Eth, AMY-2-Pro, AMY-1-But, AMY-1-Pen, and AMY-1-Hex.

4.3. Characterizations. *4.3.1. X-ray Diffraction.* Single-crystal XRD measurements were conducted on a Rigaku MicroMax-002 + CCD diffractometer using Cu Kα radiation (Rigaku, Americas). The intensity data of solvatomorphs AMY-2-Pro, AMY-1-But, AMY-1-Pen, and AMY-1-Hex were collected at 293 K.

Absorption correction and integration of the collected data were performed using the CrystalClear software package (Rigaku Americas). Crystal structures were solved by direct methods and refined through full-matrix least-square methods, which were performed using Olex 2 and SHELXS crystallography software platforms.[39,40] The hydrogen atoms were refined isotropically, and the heavy atoms were refined anisotropically. Hydrogen atoms were placed in idealized positions and refined in a riding model with U_{iso} values 1.2−1.5 times those of their parent atoms. Refinement of disorders with restraints was introduced to help data convergence.[41] Mercury software (Version 2021.2.0, Cambridge Crystallographic Data Center, United Kingdom) was used for the crystal structure and hydrogen-bonding interaction analysis.[42]

PXRD patterns were obtained using a Rigaku D/MAX-2550 diffractometer with Cu Kα radiation (Rigaku, Tokyo, Japan) operated at 45 kV and 150 mA. Samples were measured in the reflection mode in the 2θ range of 3−40° with a scan speed of 8°/min at room temperature. The theoretical powder diagrams of the solvatomorphs were calculated using Mercury software (2021.2.0), and the angular range was 3.0−40.0° (2θ) with a step size of 0.02°.

4.3.2. Thermal Analyses. DSC was recorded on a Mettler-Toledo DSC instrument (Mettler Toledo, Switzerland) and STARe Evaluation software 16.30.

TG−MS experiments were carried out on a Mettler-Toledo model TGA 1 instrument (Mettler Toledo, Switzerland) combined with a Thermostar GSD320 T3 gas analysis system (Pfeiffer Vacuum GmbH, Germany) to confirm the stoichiometry of the host and different guest solvatomorphs. Electron ionization (EI) sources were adopted in the MS system, and all samples were measured by the selected ion monitor (SIM) mode. After searching the NIST 08 (standard mass spectrometry) spectrum library, two characteristic ion mass numbers (m/z) were set for each target solvent: m/z 17, 18 for H_2O; m/z 31, 45 for ethanol; m/z 27, 45 for isopropanol; m/z 31, 56 for n-butanol; m/z 42, 55 for n-pentanol; m/z 43, 56 for n-hexanol.

Samples (5−10 mg) for the DSC and TG−MS experiments were placed in aluminum crucibles with lids, heated at 10 °C/min, and scanned in the temperature range of 35−250 °C.

4.3.3. Equilibrium Solubility in Water. The solubility in water of each solvatomorph was measured using the shake-flask method at 37 °C for 24 h and calculated by the external standard method. The absorbance of six solvatomorphs and AMY in water was determined using a Purkinje TU-1901 UV−vis spectrophotometer (Purkinje General, China), and the detection wavelength was set at 210 nm. The experiments were repeated three times.

4.4. Theoretical Computation. The contact and solvent-accessible surfaces of water and other solvent molecules were analyzed using Mercury software (2021.2.0). The probe radius was 0.8 A, and grid spacing was 0.3 A, respectively. The intermolecular interaction energy and EDA based on SAPT were determined by using the PSI4 1.4 program,[43] and the level of calculation was SAPT0/jun-cc-pVDZ.[44] All molecules (including AMY, water molecules W_1 and W_2, and the third molecule W_3 or S_3) in each asymmetric unit were optimized, and the single point energies were calculated by DFT. Geometry optimizations of all hydrogen atoms and single-energy calculations of solvatomorphs were conducted by DFT using the Gaussian 16 package under the B3LYP-D3/6-311G (d, p) level and the M06-2X/def2-TZVP level, respectively.[45,46] The basis set superposition error was calculated at the same level

using the full counterpoise procedure, and the pairwise interaction energies were then extracted from the calculated results. All of the heavy atoms were at original X-ray coordinates. The Multiwfn 3.8 package was used to extract the local maxima and minima from the MEPS mapped onto the 0.002 Bohr $°A^{-3}$ electron density isosurface.[47] The AMY solvatomorphs' crystal-packing similarities were analyzed quantitatively using the XPac 2.0.2[48,49] software. Also, the CrystalExplorer software 17.5 was used for displaying Hirshfeld surfaces analysis.[50]

4.5. Transformation Test. Transformations between the solvatomorphs were carried out using the solvent replacement method and thermal method. Inversion of AMY to AMY-W or alcohol hydrates: excess amounts of AMY were suspended in a water-acetonitrile mixture (1:1, v/v), ethanol, isopropanol-acetonitrile mixture (1:1, v/v), n-butanol−acetonitrile mixture (1:1, v/v), n-pentanol−acetonitrile mixture (1:1, v/v), and n-hexanol−acetonitrile mixture (1:1, v/v) separately at room temperature with a constant stirring rate for one day. The suspensions were filtered and air-dried at room temperature to obtain the corresponding solvatomorphs. In addition, AMY also transformed to AMY-W under high humidity conditions (25−30 °C and 92.5% RH for 10 days).

Inversion from AMY-W to alcohol dihydrates: excess amounts of AMY-W were suspended in ethanol, isopropanol−acetonitrile mixture (1:1, v/v), n-butanol−acetonitrile mixture (1:1, v/v), n-pentanol−acetonitrile mixture (1:1, v/v), and n-hexanol−acetonitrile mixture (1:1, v/v) separately at room temperature with a constant stirring rate for one day. The suspensions were filtered and air-dried at room temperature to obtain the corresponding forms.

Inversion of alcohol dihydrates to AMY-W: excess amounts of AMY-Eth, AMY-2-Pro, AMY-1-But, AMY-1-Pen, and AMY-1-Hex samples were weighed, and a water-acetonitrile mixture (1:1, v/v) solvent was added. The following steps are the same as above.

Inversion of AMY-W or alcohol hydrates to AMY: AMY-W, AMY-Eth, AMY-2-Pro, AMY-1-But, AMY-1-Pen, and AMY-1-Hex samples, was performed by heating at 170 °C for 10 min.

ASSOCIATED CONTENT

Supporting Information
The Supporting Information is available free of charge at https://pubs.acs.org/doi/10.1021/acsomega.1c07314.

Crystallographic data of six solvatomorphs of AMY, parameters (Å, degree) of main hydrogen bondings for AMY-2-Pro, AMY-1-Pen, and AMY-1-Hex, TG calculation results of six solvatomorphs of AMY, interaction energies and EDA of W_1, interaction energies and EDA of W_2, interaction energies and EDA of W_3 and S_3, XPac analysis of solvatomorphs of AMY, contact and solvent-accessible surfaces of AMY solvatomorphs, IR spectra for six solvatomorphs of AMY, and experiment and the result parts of the infrared spectroscopy Analysis(PDF)
Crystallographic data for CCDC 2128815 (CIF)
Crystallographic data for CCDC 2128827 (CIF)
Crystallographic data for CCDC 2128825 (CIF)

AUTHOR INFORMATION

Corresponding Authors
Dezhi Yang − *Beijing City Key Laboratory of Polymorphic Drugs, Center of Pharmaceutical Polymorphs, Institute of Materia Medica, Chinese Academy of Medical Sciences and Peking Union Medical College, Beijing 100050, China;* orcid.org/0000-0002-3159-4126; Email: ydz@imm.ac.cn

Yang Lu − *Beijing City Key Laboratory of Polymorphic Drugs, Center of Pharmaceutical Polymorphs, Institute of Materia Medica, Chinese Academy of Medical Sciences and Peking Union Medical College, Beijing 100050, China;* orcid.org/0000-0002-2274-5703; Phone: +86 106315212; Email: luy@imm.ac.cn; Fax: +86 1063165212

Guanhua Du − *Beijing City Key Laboratory of Drug Target Identification and Drug Screening, Institute of Materia Medica, Chinese Academy of Medical Sciences and Peking Union Medical College, Beijing 100050, China;* Email: dugh@imm.ac.cn

Authors
Tingting Zhang − *Beijing City Key Laboratory of Polymorphic Drugs, Center of Pharmaceutical Polymorphs, Institute of Materia Medica, Chinese Academy of Medical Sciences and Peking Union Medical College, Beijing 100050, China;* orcid.org/0000-0003-2808-0658

Shiying Yang − *Beijing City Key Laboratory of Polymorphic Drugs, Center of Pharmaceutical Polymorphs, Institute of Materia Medica, Chinese Academy of Medical Sciences and Peking Union Medical College, Beijing 100050, China*

Baoxi Zhang − *Beijing City Key Laboratory of Polymorphic Drugs, Center of Pharmaceutical Polymorphs, Institute of Materia Medica, Chinese Academy of Medical Sciences and Peking Union Medical College, Beijing 100050, China*

Complete contact information is available at:
https://pubs.acs.org/10.1021/acsomega.1c07314

Notes
The authors declare no competing financial interest.

REFERENCES
(1) Fukuda, T.; Ito, H.; Yoshida, T. Glycosides and their quantitative HPLC analysis of commercial Persicae semen. *Nat. Med.* **2003**, *57*, 18−22.

(2) Tanaka, R.; Nitta, A.; Nagatsu, A. Application of a quantitative 1H-NMR method for the determination of amygdalin in Persicae semen, Armeniacae semen, and Mume fructus. *J. Nat. Med.* **2014**, *68*, 225−230.

(3) Nielsen, K. A.; Olsen, C. E.; Pontoppidan, K.; Møller, B. L. Leucine-derived cyano glucosides in barley. *Plant Physiol.* **2002**, *129*, 1066−1075.

(4) Zagrobelny, M.; Bak, S.; Rasmussen, A. V.; Jørgensen, B.; Naumann, C. M.; Lindberg Møller, B. Cyanogenic glucosides and plant-insect interactions. *Phytochemistry* **2004**, *65*, 293−306.

(5) Moradipoodeh, B.; Jamalan, M.; Zeinali, M.; Fereidoonnezhad, M.; Mohammadzadeh, G. In vitro and in silico anticancer activity of amygdalin on the SK-BR-3 human breast cancer cell line. *Mol. Biol. Rep.* **2019**, *46*, 6361.

(6) Ayaz, Z.; Zainab, B.; Khan, S.; Abbasi, A. M.; Elshikh, M. S.; Munir, A.; Al-Ghamdi, A. A.; Alajmi, A. H.; Alsubaie, Q. D.; Mustafa, A. E.-Z. M. A. In silico authentication of amygdalin as a potent anticancer compound in the bitter kernels of family Rosaceae. *Saudi J. Biol. Sci.* **2020**, *27*, 2444−2451.

(7) Miyagoshi, M.; Amagaya, S.; Ogihara, Y. Antitussive Effects of L-Ephedrine, Amygdalin, and Makyokansekito (Chinese Traditional Medicine) using a Cough Model Induced by Sulfur Dioxide Gas in Mice. *Planta Med.* **1986**, *52*, 275−278.

(8) Hwang, H.-J.; Kim, P.; Kim, C.-J.; Lee, H.-J.; Shim, I.; Yin, C. S.; Yang, Y.; Hahm, D.-H. Antinociceptive Effect of Amygdalin Isolated from Prunus armeniaca on Formalin-Induced Pain in Rats. *Biol. Pharm. Bull.* 2008, 31, 1559−1564.

(9) Mirmiranpour, H.; Khaghani, S.; Zandieh, A.; Khalilzadeh, O.; Gerayesh-Nejad, S.; Morteza, A.; Esteghamati, A. Amygdalin inhibits angiogenesis in the cultured endothelial cells of diabetic rats. *Indian J. Pathol. Bacteriol.* 2012, 55, 211−214.

(10) Zhang, X.; Hu, J.; Zhuo, Y.; Cui, L.; Li, C.; Cui, N.; Zhang, S. Amygdalin improves microcirculatory disturbance and attenuates pancreatic fibrosis by regulating the expression of endothelin-1 and calcitonin gene-related peptide in rats. *J. Chin. Med. Assoc.* 2018, 81, 437−443.

(11) Chang, H.-K.; Yang, H.-Y.; Lee, T.-H.; Shin, M.-C.; Lee, M.-H.; Shin, M.-S.; Kim, C.-J.; Kim, O.-J.; Hong, S.-P.; Cho, S. Armeniacae semen Extract Suppresses Lipopolysaccharide-Induced Expressions of Cycloosygenase-2 and Inducible Nitric Oxide Synthase in Mouse BV2 Microglial Cells. *Biol. Pharm. Bull.* 2005, 28, 449−454.

(12) Eriksson, L.; Widmalm, G. Amygdalin trihydrate. *Acta Acta Crystallogr., Sect. E: Crystallogr. Commun.* 2005, 61, o860.

(13) Nangia, A.; Desiraju, G. R. Pseudopolymorphism: Occurrences of hydrogen bonding organic solvents in molecular crystals. *Chem. Commun.* 1999, 7, 605−606.

(14) Haleblian, J.; McCrone, W. Pharmaceutical applications of polymorphism. *J. Pharm. Sci.* 1969, 58, 911−929.

(15) Bingham, A. L.; Hughes, D. S.; Hursthouse, M. B.; Lancaster, R. W.; Tavener, S.; Threlfall, T. L. Over one hundred solvates of sulfathiazole. *Chem. Commun.* 2001, 7, 603−604.

(16) Xu, W.; Gong, N.; Yang, S.; Zhang, N.; He, L.; Du, G.; Lu, Y. Isostructurality Among Solvates of Cabazitaxel: X-ray Structures and New Solvates Preparation. *J. Pharm. Sci.* 2015, 104, 1256−1262.

(17) Raemakers, K. G. H.; Bart, J. C. J. Applications of simultaneous thermogravimetry-mass spectrometry in polymer analysis. *Thermochim. Acta* 1997, 295, 1−58.

(18) Yuan, P.-H.; Bi, Y.-C.; Su, B.; Yang, D.-Z.; Gong, N.-B.; Zhang, L.; Lu, Y.; Du, G.-H. Analysis of Four Solvatomorphs of Betulin by TG-DTA-EI/PI-MS System Equipped with the Skimmer-Type Interface. *Nat. Prod. Bioprospect.* 2020, 10, 141−152.

(19) Paulose, S.; Thomas, D.; Jayalatha, T.; Rajeev, R.; George, B. K. TG−MS study on the kinetics and mechanism of thermal decomposition of copper ethylamine chromate, a new precursor for copper chromite catalyst. *J. Therm. Anal. Calorim.* 2016, 124, 1099−1108.

(20) Sugimoto, K.; Dinnebier, R. E.; Zakrzewski, M. Structural characterization of anhydrous naloxone- and naltrexone hydrochloride by high resolution laboratory X-ray powder diffraction and thermal analysis. *J. Pharm. Sci.* 2007, 96, 3316−3323.

(21) Pratt, L. M.; Truhlar, D. G.; Cramer, C. J.; Kass, S. R.; Thompson, J. D.; Xidos, J. D. Aggregation of Alkyllithiums in Tetrahydrofuran. *J. Org. Chem.* 2007, 72, 2962−2966.

(22) Grimme, S.; Antony, J.; Ehrlich, S.; Krieg, H. A consistent and accurate ab initio parametrization of density functional dispersion correction (DFT-D) for the 94 elements H-Pu. *J. Chem. Phys.* 2010, 132, 154104.

(23) Murray, J. S.; Politzer, P. The electrostatic potential: an overview. *Wiley Interdiscip. Rev.: Comput. Mol. Sci.* 2011, 1, 153−163.

(24) Jia, L.; Zhou, L.; Du, W.; Zhou, L.; Zhang, M.; Hou, B.; Bao, Y.; Wang, Z.; Yin, Q. Simultaneous Effects of Multiple Factors on Solution-Mediated Phase Transformation: A Case of Spironolactone Forms. *Org. Process Res. Dev.* 2018, 22, 836−845.

(25) Jiang, C.; Yan, J.; Wang, Y.; Zhang, J.; Wang, G.; Yang, J.; Hao, H. Isolation Strategies and Transformation Behaviors of Spironolactone Forms. *Ind. Eng. Chem. Res.* 2015, 54, 11222−11229.

(26) Chennuru, R.; Muthudoss, P.; Voguri, R. S.; Ramakrishnan, S.; Vishweshwar, P.; Babu, R. R. C.; Mahapatra, S. Iso-Structurality Induced Solid Phase Transformations: A Case Study with Lenalidomide. *Cryst. Growth Des.* 2017, 17, 612−628.

(27) Galek, P. T. A.; Fábián, L.; Allen, F. H. Persistent hydrogen bonding in polymorphic crystal structures. *Acta Crystallogr., Sect. B: Struct. Sci., Cryst. Eng. Mater.* 2009, 65, 68−85.

(28) Ranjan, S.; Devarapalli, R.; Kundu, S.; Saha, S.; Deolka, S.; Vangala, V. R.; Reddy, C. M. Isomorphism: "molecular similarity to crystal structure similarity" in multicomponent forms of analgesic drugs tolfenamic and mefenamic acid. *IUCrJ* 2020, 7, 173−183.

(29) Samie, A.; Desiraju, G. R.; Banik, M. Salts and Cocrystals of the Antidiabetic Drugs Gliclazide, Tolbutamide, and Glipizide: Solubility Enhancements through Drug−Coformer Interactions. *Cryst. Growth Des.* 2017, 17, 2406−2417.

(30) Venkataramanan, N. S.; Suvitha, A.; Kawazoe, Y. Density functional theory study on the dihydrogen bond cooperativity in the growth behavior of dimethyl sulfoxide clusters. *J. Mol. Liq.* 2018, 249, 454−462.

(31) Liu, Q.; Yang, D.; Chen, T.; Zhang, B.; Xing, C.; Zhang, L.; Lu, Y.; Du, G. Insights into the Solubility and Structural Features of Four Praziquantel Cocrystals. *Cryst. Growth Des.* 2021, 21, 6321−6331.

(32) Wu, D.; Li, J.; Xiao, Y.; Ji, X.; Li, C.; Zhang, B.; Hou, B.; Zhou, L.; Xie, C.; Gong, J.; Chen, W. New Salts and Cocrystals of Pymetrozine with Improvements on Solubility and Humidity Stability: Experimental and Theoretical Study. *Cryst. Growth Des.* 2021, 21, 2371−2388.

(33) Wang, R.; Yuan, P.; Yang, D.; Zhang, B.; Zhang, L.; Lu, Y.; Du, G. Structural features and interactions of new sulfamethazine salt and cocrystal. *J. Mol. Struct.* 2021, 1229, 129596.

(34) Yang, D.; Wang, H.; Liu, Q.; Yuan, P.; Chen, T.; Zhang, L.; Yang, S.; Zhou, Z.; Lu, Y.; Du, G. Structural landscape on a series of rhein: Berberine cocrystal salt solvates: The formation, dissolution elucidation from experimental and theoretical investigations. *Chin. Chem. Lett.* 2021, DOI: 10.1016/j.cclet.2021.10.012.

(35) Spackman, M. A.; Jayatilaka, D. Hirshfeld surface analysis. *CrystEngComm* 2009, 11, 19−32.

(36) Spackman, M. A.; McKinnon, J. J. Fingerprinting intermolecular interactions in molecular crystals. *CrystEngComm* 2002, 4, 378−392.

(37) McKinnon, J. J.; Jayatilaka, D.; Spackman, M. A. Towards quantitative analysis of intermolecular interactions with Hirshfeld surfaces. *Chem. Commun.* 2007, 37, 3814−3816.

(38) Jia, L.; Zhang, S.; Yang, W.; Bao, Y.; Hou, B.; Zhou, L.; Yin, Q. Insights into Intermolecular Interactions of Spironolactone Solvates. *Cryst. Growth Des.* 2021, 21, 3677−3688.

(39) Sheldrick, G. M. A Short History of ShelX. *Acta Crystallogr., Sect. A: Found. Crystallogr.* 2008, 64, 112−122.

(40) Dolomanov, O. V.; Bourhis, L. J.; Gildea, R. J.; Howard, J. A. K.; Puschmann, H. OLEX2: a complete structure solution, refinement and analysis program. *J. Appl. Crystallogr.* 2009, 42, 339−341.

(41) Muller, P.; Herbst, R. *Crystal Structure Refinement*; Springer: US, 2005.

(42) Macrae, C. F.; Edgington, P. R.; McCabe, P.; Pidcock, E.; Shields, G. P.; Taylor, R.; Towler, M.; van de Streek, J. Mercury: visualisation and analysis of crystal structures. *J. Appl. Crystallogr.* 2006, 39, 453.

(43) Smith, D. G. A.; Burns, L. A.; Simmonett, A. C.; Parrish, R. M.; Schieber, M. C.; Galvelis, R.; Kraus, P.; Kruse, H.; Di Remigio, R.; Alenaizan, A.; James, A. M.; Lehtola, S.; Misiewicz, J. P.; Scheurer, M.; Shaw, R. A.; Schriber, J. B.; Xie, Y.; Glick, Z. L.; Sirianni, D. A.; O'Brien, J. S.; Waldrop, J. M.; Kumar, A.; Hohenstein, E. G.; Pritchard, B. P.; Brooks, B. R.; Schaefer, H. F.; Sokolov, A. Y.; Patkowski, K.; DePrince, A. E.; Bozkaya, U.; King, R. A.; Evangelista, F. A.; Turney, J. M.; Crawford, T. D.; Sherrill, C. D. PSI4 1.4: Open-source software for high-throughput quantum chemistry. *J. Chem. Phys.* 2020, 152, 184108.

(44) Parker, T. M.; Burns, L. A.; Parrish, R. M.; Ryno, A. G.; Sherrill, C. D. Levels of symmetry adapted perturbation theory (SAPT). I. Efficiency and performance for interaction energies. *J. Chem. Phys.* 2014, 140, 094106.

(45) Frisch, M.; Trucks, G.; Schlegel, H.; Scuseria, G.; Robb, M.; Cheeseman, J.; Scalmani, G.; Barone, V.; Petersson, G.; Nakatsuji, H. *Gaussian 16*, Revision A.03; Gaussian, Inc.: Wallingford, CT, 2016.

(46) Vener, M. V.; Levina, E. O.; Koloskov, O. A.; Rykounov, A. A.; Voronin, A. P.; Tsirelson, V. G. Evaluation of the Lattice Energy of the

Two-Component Molecular Crystals Using Solid-State Density Functional Theory. *Cryst. Growth Des.* **2014**, *14*, 4997−5003.

(47) Lu, T.; Chen, F. Multiwfn: A multifunctional wavefunction analyzer. *J. Comput. Chem.* **2012**, *33*, 580−592.

(48) Gelbrich, T.; Hursthouse, M. B. Systematic investigation of the relationships between 25 crystal structures containing the carbamazepine molecule or a close analogue: a case study of the XPac method. *CrystEngComm* **2006**, *8*, 448−460.

(49) Fabbiani, F. P. A.; Dittrich, B.; Florence, A. J.; Gelbrich, T.; Hursthouse, M. B.; Kuhs, W. F.; Shankland, N.; Sowa, H. Crystal structures with a challenge: high-pressure crystallisation of ciprofloxacin sodium salts and their recovery to ambient pressure. *CrystEngComm* **2009**, *11*, 1396−1406.

(50) Jayatilaka, D.; Wolff, S.; Grimwood, D.; McKinnon, J.; Spackman, M. CrystalExplorer: A tool for displaying Hirshfeld surfaces and visualising intermolecular interactions in molecular crystals. *Acta Crystallogr., Sect. A: Found. Adv.* **2006**, *62*, s90.